Large-Area Artificial van der Waals "Mille-Feuille" Superlattices

Hao Wei, Simon Dubois, Frederic Brunnett, Julian Peiro, Florian Godel, Cécile Carrétéro, Federico Panciera, Sophie Collin, Fayçal Bouamrane, Victor Zatko, et al.

ADVANCED MATERIALS INTERFACES
Open Access
www.advmatinterfaces.de

Large-Area Artificial van der Waals "Mille-Feuille" Superlattices

Hao Wei, Simon Dubois, Frederic Brunnett, Julian Peiro, Florian Godel, Cécile Carrétéro, Federico Panciera, Sophie Collin, Fayçal Bouamrane, Victor Zatko, Marta Galbiati, Etienne Carré, Gilles Patriarche, Frédéric Petroff, Jean-Christophe Charlier, Marie-Blandine Martin, Bruno Dlubak, and Pierre Seneor**

Van der Waals heterostructures are set as strong contenders for post-CMOS quantum materials engineering. A major step for their systematic exploration and exploitation of technological component demonstrators resides in their eased large-scale design. In this direction, the growth of artificial van der Waals 2D superlattices is presented here such as $(MoS_2/WS_2)_n$, $(WS_2/WSe_2)_n$, and $(MoS_2/WSe_2)_n$ with unit cells repetitions reaching $n > 10$. The fabrication of these materials is enabled by a fully automated in-situ pulsed laser deposition (PLD) tool. This approach provides cm^2 scale homogeneous superlattices with on-demand material parameters tailoring (layer number, order, and composition). The process is rapid and simple compared to manual pickup exfoliation methods or to sequential transfers of single layers grown by techniques such as chemical vapor deposition, allowing a large repetition of the unit cells in a "mille-feuille" cake configuration. The computational exploration of this family of superlattice materials sheds light on the potential for optoelectronic property design by shaping the band-structure landscape while taking into account the influential effects induced by proximity. Overall, this large-area approach is proposed as an entry point for the systematic design of complex van der Waals heterostructures.

1. Introduction

2D materials and their van der Waals heterostructures are widely foreseen as strong contenders for "more than Moore" enhanced Complementary Metal-Oxyde-Semiconductor (CMOS+X) technologies, as well as beyond-CMOS technologies including spintronics, photonics, neuromorphic and quantum computations.[1–7] Indeed 2D materials offer epitaxy-free heterostructure definition at ultimate atomic thicknesses, as well as extreme tailoring in terms of composition and associated properties. Beyond the zero-gap Dirac band structure of graphene, and the relatively large gap h-BN 2D insulator, an extensive library of 2D semiconductors is now being explored and rationalized.[8–11] This exploration encompasses elemental materials (such as black phosphorus, silicene, and germanene) as well as more complex layered compounds (such as mono-, bi-, and trichalcogenides). The properties of these systems depend not only on their composition but also on their stacking configuration, owing to the proximity effects amplified by their 2D nature.[12] This diversity allows for a versatile toolkit for the fabrication of tailored 2D heterostructures.[13] Additionally, these materials exhibit intriguing phenomena such as "magic-angle" moiré-induced superconductivity or ferroelectricity, as well as topologically protected states.[14–18] Already, discrete functions based on these materials have been demonstrated (such as

H. Wei, F. Brunnett, J. Peiro, F. Godel, C. Carrétéro, S. Collin, F. Bouamrane, V. Zatko, M. Galbiati, E. Carré, F. Petroff, M.-B. Martin, B. Dlubak, P. Seneor
Laboratoire Albert Fert, CNRS, Thales
Université Paris-Saclay
Palaiseau 91767, France
E-mail: bruno.dlubak@cnrs-thales.fr; pierre.seneor@cnrs-thales.fr

The ORCID identification number(s) for the author(s) of this article can be found under https://doi.org/10.1002/admi.202400409

S. Dubois, J.-C. Charlier
Institute of Condensed Matter and Nanosciences (IMCN)
Université Catholique de Louvain
Louvain-la-Neuve B-1348, Belgium

F. Panciera, G. Patriarche
Centre de Nanosciences et de Nanotechnologies
Université Paris-Saclay, CNRS
Palaiseau 91120, France

DOI: 10.1002/admi.202400409

antennae, RF switches, photo-detectors and sensors, light emitter, image sensors...) along with the first steps toward high integration densities and logic circuits.[19,20] Sustaining this applicative vision, first pilot lines including 2D materials have been reported using production tools,[16,21,22] establishing the basic conditions for their growth, integration, and stabilization in functional structures.[23,24] In this context, the exploration of complex van der Waals heterostructures of 2D materials, reminiscent of the original enthusiasm toward III-V semiconductors,[25–27] are being actively pursued to make full use of the unique properties of this class of highly tailorable, ultimately thin materials.[28,29] This opens a very promising path for disruptive concepts to emerge from this large quantum materials platform.

Paramount progress has been achieved in deriving 2D materials and in turn fueling the exploration of their properties. Following the initial success of exfoliation,[30] the subsequent stacking of these 2D layers into heterostructures has however come with great challenges.[31–33] The first pioneering approach consisted of extending the mechanical exfoliation technique with a micro-controlled polymer stamp-based pick-up assembly.[34,35] This process allowed the combination of different exfoliated 2D flakes in a given stack, leading to the successful exploitation of relatively simple heterostructures.[14,36–38] This manual approach has been instrumental in discovering the fascinating fundamental properties of van der Waals heterostructures.[39] However, its reach in terms of heterostructure complexity has been limited as the mechanical stacking steps of micron-sized flakes have proven to be particularly tedious and time-consuming with a non-negligeable risk of failure for each additional stamping step. In parallel, large-scale growths of 2D materials have been steadily developed, particularly by chemical vapor deposition (CVD).[40–42] Stacking CVD-grown 2D layers by successive wet-transfers allows to reach large-scale stacks, but again at the cost of ex situ mechanical transfers.[43] It is worth noting, in addition, that when manipulations in wet or ambient conditions are involved, the insertion of sensitive 2D materials (this concerns a large set of 2D crystals) is ultimately excluded.[44–46] Pioneering works[47,48] have demonstrated stacking of 2–3 large 2D layers establishing simple heterostructures already with stark perspectives. Still, these results call for dedicated in-situ simpler and faster assembly, drawing from recent advances demonstrated for a few 2D layers with direct growth techniques such as CVD, pulsed laser deposition (PLD), or molecular beam epitaxy (MBE).[44,49–53] Indeed the community is now aiming toward van der Waals heterostructures with higher complexity and a much larger repetition count of 2D layer stacking as required for envisioned exploitation.[4] Following an initial proposal by Esaki and Tsu in the 70s,[54] superlattices built out of structured and repeated quantum wells are fundamental for numerous optoelectronic properties and already led to applications such as quantum cascade lasers, light emitting diodes, photodetectors, HFETs for high-frequency low-noise amplifiers, Bragg mirrors for single photon sources in quantum dots...[25–27,55–58] While these are now well mastered with III-V semiconductors, they are particularly difficult to fabricate with 2D materials. Even though the field of 2D materials has been advancing for >15 years, the creation of such superlattices remains unachieved. This underscores the significant challenge in building and accessing complex tailored quantum van der Waals heterostructure platforms to systematically explore their vast potential.

In the following, we present a fabrication process allowing the assembly of complex van der Waals heterostructures, illustrated by the study of several reference superlattices of transition metal dichalcogenides (TMD) 2D semiconductors. We derive stacks of 20 alternates of TMD layers on cm^2 scale samples by direct in-situ PLD, analyzed by Scanning Transmission Electron Microscopy (STEM), Energy Dispersive X-ray (EDX), X-ray photoelectron Spectroscopy (XPS), and Raman spectroscopy. With the aim to highlight the potential that arises from tailoring these structures through hybridized heterointerfaces, we present an initial discussion of the expected band structures within this family of artificial nanolayered superlattice van der Waals materials. The calculations presented here serve as a means to illustrate the importance of proximity effects when stacking 2D layers together as one should not simply expect juxtaposition of disjoint 2D semiconductors properties. The enhanced flexibility introduced by our approach, not only in terms of the composition of the 2D materials' unit cells but also in the repetition parameters, offers an entry point for the systematic design and exploration of highly complex functional van der Waals superlattices.

2. Results and Discussion

The growth setup is a customized TSST PLD system with a base pressure of 10^{-8} mbar.[44] A 355 nm Nd:YAG laser (tripled frequency) is used to shoot the bulk material targets. We carry the growth sequences using automated in-situ target switching to enable the progressive build-up of composite superlattices (see **Figure 1**). We focus here on reference WS_2, MoS_2, and WSe_2 2D semiconductor materials. The stoichiometric targets (Neyco) are prepared prior to deposition by being systematically pre-ablated in the PLD chamber under growth conditions for 5 min, without exposing the sample. The sample, a SiO_2(90 nm)/Si substrate, is then preheated at 400 °C in 0.1 mbar Ar for 5 min. Importantly we set the sample-to-target distance to 70 mm to allow a 2D-mode growth away from the most energetic part of the ablation plume.[53] For each 2D semiconductor layer, the corresponding target is shot during 20s, corresponding to the required time for bilayer growth.[44] We fabricate superlattices with 20 alternate 2D semiconductor stacks, corresponding to 10 unit cells of WS_2/MoS_2. Including the target swap idle time, corresponds to a fabrication time of ≈30 min for the realization of this extreme 2D material stacking under the specific conditions of our setup. The fabrication process is hence considerably faster than any possible manual stacking technique, with unparalleled reproducibility and access to much higher complexity.

To probe the proper formation of the 2D superlattice we perform cross-sectional STEM observations as presented in **Figure 2**. First, a lamella is prepared based on carbon and Pt-capped samples using focused ion beam (FIB) micromachining. A Themis STEM setup from ThermoFicher Scientific, also equipped with a Super-X EDX detector, is used to acquire the STEM images (200 kV) and the EDX line scans. A typical representative image of a section of the superlattice is presented for two different runs in Figure 2a,b. We observe the lamellar organization of the heterostructure showing long-range crystallization and a z-axis stacking as expected from the processes described above.

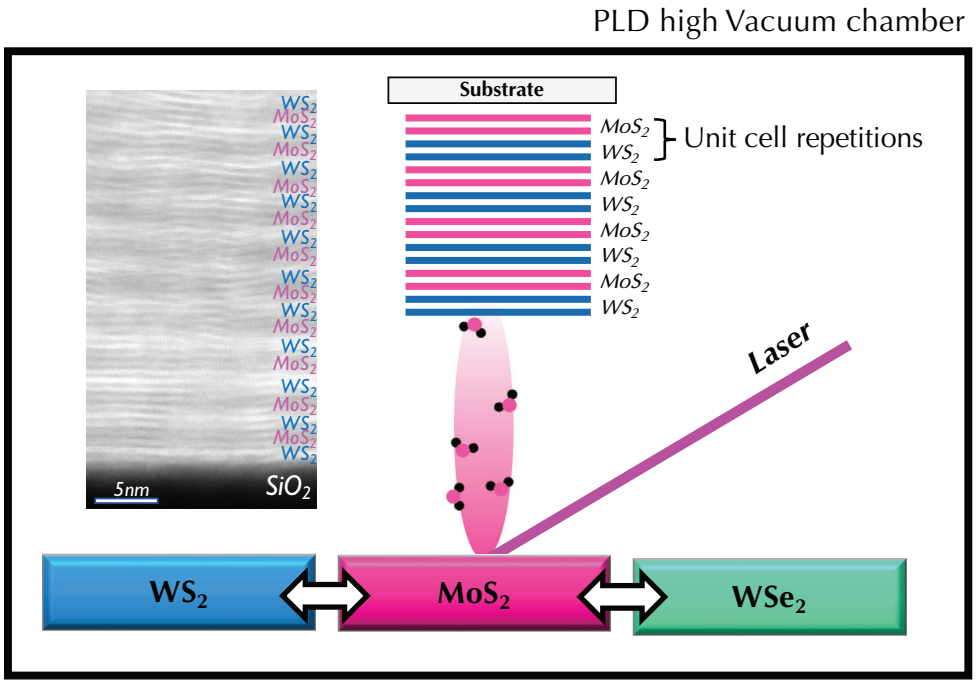

Figure 1. In situ direct assembly of 2D semiconductor unit cells into tailored superlattice material, in a configuration reminiscent of the "mille-feuille" European pastry. Schematic representation of the pulsed laser deposition (PLD) growth approach with in-situ automatized material target switching. The inset presents a lateral section of a typical 2D superlattice as observed through STEM HAADF (scanning transmission electron microscope high-angle annular dark-field imaging).

The clear and homogeneous unit-cell repetition already shows the high repeatability of the PLD approach, with a result barely achievable by manual stacking such as pickup or wet transfers. Figure 2a shows a run where MoS_2 and WS_2 bilayers are alternated into a stack of ≈10 unit cells. The precise composition of this 2D heterostructure can be subtly tailored as shown in Figure 2b, where a second run leads to a more complex unit cell embedding 3 additional WS_2 layers. This illustrates the flexibility of the PLD growth approach to define 2D heterostructures well suited for fine adaptation to targeted application requirements.

A fast Fourier transform (FFT) analysis of the high-resolution STEM images allows us to confirm more precisely the crystalline structure of these growths. We observe a 2.8 nm WS_2/MoS_2 period for the run of Figure 2a (corresponding to a 2 + 2 TMD unit cells) and 4.9 nm in the case of Figure 2b (corresponding to a 5 + 2 TMD unit cells). In addition, a second FFT peak is observed corresponding in both cases to the 2D-plane interlayer spacing with the expected 0.7 nm period for TMDs compounds. This already demonstrates the success of building a 2D superlattice heterostructure.

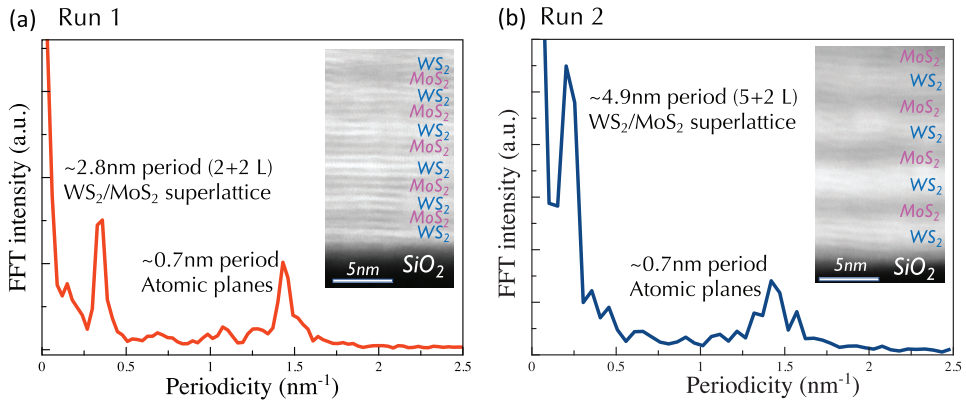

Figure 2. FFT analysis of 2D superlattices lateral section as observed through STEM HAADF. Depending on run conditions, the resulting superlattice structure is varied: compared to run 1 in panel a), 3 additional WS_2 layers are grown in the presented run 2 in panel b). This highlights the potential to finely tune the organization of mille-feuille superlattice quantum materials properties by selecting growth parameters. This analysis reveals the organization of the superlattice showing atomic plane periods of the layered 2D materials in use (0.7 nm period) as well as the longer-range organization with the crafted unit cell of 2D semiconductors (2.8 and 4.9 nm periods respectively).

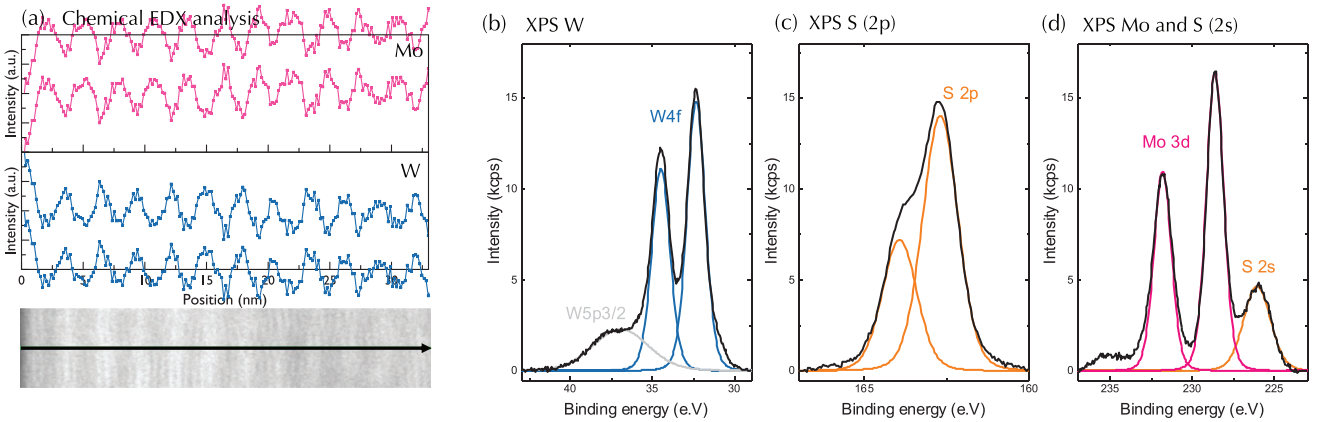

Figure 3. Chemical analysis of a tailored 2D $(MoS_2/WS_2)_n$ superlattice material. We present both analyses by a) Energy-dispersive X-ray spectroscopy (EDX) line scan and b,c,d) X-ray photoelectron spectroscopy (XPS) measurements of the main elemental signatures of the superlattice materials. The combined EDX and XPS analysis highlights the alternate of crystalized MoS_2 and WS_2 2D semiconductors in the fabricated superlattices.

We further expose below the chemical and crystallographic compositions of these heterostructures by combined EDX, XPS, and Raman spectroscopy analyses. In this direction, we carry a complementary STEM cross-section chemical analysis by EDX spectroscopy to highlight the alternating chemical composition of these superlattices. The analyses of the EDX data in **Figure 3**a highlight the periodic alternance of W and Mo atoms in the TMDs 2D semiconductors structure with the expected 2.8 nm period confirming our FFT analysis (Figure 2). To further assess their crystalline and chemical state we carry out XPS and Raman spectroscopy studies. Regarding the XPS study, we collect spectra of core levels of W 4f, Mo 3d, and S 2p with a pass energy of 30 eV, using a Mg X-ray source of the Omicron setup. The XPS spectra are displayed in Figure 3 and confirm the expected stoichiometry of each TMD embedded in the artificial heterostructures. Following Loh et al.,[59] we are indeed able to identify the chemical attributes of the TMDs layers. Focusing on WS_2 signatures: S^{2-} states of S atoms in WS_2 with energy splitting of 1.2 eV are observed (Figure 3c), as well as specific W^{4+} states (Figure 3b). These are the signatures of crystalline 2H-WS_2 in a hexagonal semiconductor phase.[59] From these XPS spectra, we further extract a W:S ratio of ~0.5 expected regarding WS_2 TMD stoichiometry. Similar conclusions can be made for MoS_2 (Figure 3c,d). The measured XPS data in these complex heterostructures thus capture the chemical environments of S, W, and Mo atoms expected in MoS_2 and WS_2 2D crystals. Finally, as an additional experiment, we carry out Raman characterizations using a Renishaw spectrometer with a 514 nm laser (**Figure 4**) as MoS_2, WS_2, and other TMDs give identifiable Raman signatures.[60,61] We display a typical spectrum obtained on the superlattice material in Figure 4b, revealing the combined signatures of both MoS_2 and WS_2 crystals: MoS_2 2LA + $E^1{}_{2g}$ modes, WS_2 2LA + E_{2g} modes, as well as the MoS_2 and WS_2 A_{1g}/A1′ modes.

Overall, these different characterizations demonstrate the fabrication of a 2D semiconductor-based van der Waals superlattice, based on a direct and automated process unlocking high complexity and the extreme repetition of unit cells. This highlights the strong potential of the PLD approach to build layered artificial crystals with tailored levels of complexity.

We now explore the large-scale homogeneity of these complex heterostructures. As discussed above, the main difficulty for the fabrication of van der Waals heterostructures is their controlled reproducible stacking at sample scales. The controlled transfer of CVD layers has been well explored but remains tedious and unpracticable beyond a few stacked layers in terms of time scales and probability of success.[43] Furthermore, this is mostly an ex-situ process involving exposition to the uncontrolled atmosphere and etching solutions as well as transfer polymers. Here we fabricate the entire complex heterostructure in a single run. Optically, the resulting cm^2 samples are highly homogeneous (Figure 4a). We further probe the resulting layers by Raman spectroscopy as presented in Figure 4. It appears that the whole surface of the sample is covered by the 2D materials heterostructure with characteristic peaks of MoS_2 and WS_2 appearing similarly at all locations of the sample. We plot in Figure 4c,d a large mapping of the intensity of characteristic MoS_2 and WS_2 Raman modes over the whole cm^2 sample to highlight the homogeneity of the large-scale coverage. Overall, these measurements show that the resulting growth is homogenous over the size of our sample, leading to a cm^2 complex van der Waals heterostructure, to be compared to the usual μm^2 surface range of exfoliated flakes. This result is particularly striking, as it shows how PLD offers complex stackings of 2D materials on large scales with high flexibility.

Illustratively, we have further extended this study to other artificial heterostructures such as $(WS_2/WSe_2)_n$, $(MoS_2/WSe_2)_n$ (and even a more complex $(WS_2/MoS_2/WSe_2)_n$ unit cell) with similar results. As presented in **Figure 5** we have acquired 45 × 45 μm^2 Raman mappings for different systems, and the different stacks result in combined Raman signatures that are observed homogeneously on the samples. Strikingly, the tracking of the Raman signatures for WS_2, WSe_2, and MoS_2 reveals a particularly high and reproducible homogeneity of each stacked material layer for the different studied 2D superlattices. These results further assess the potential of the proposed PLD technique to finely tailor complex 2D heterostructures with high flexibility, and in turn define large families of artificial van der Waals materials.

We purposively focus here on illustrative superlattice heterostructures as these are both complex in nature (with required repetitive growth of well-controlled ultra-thin films) and

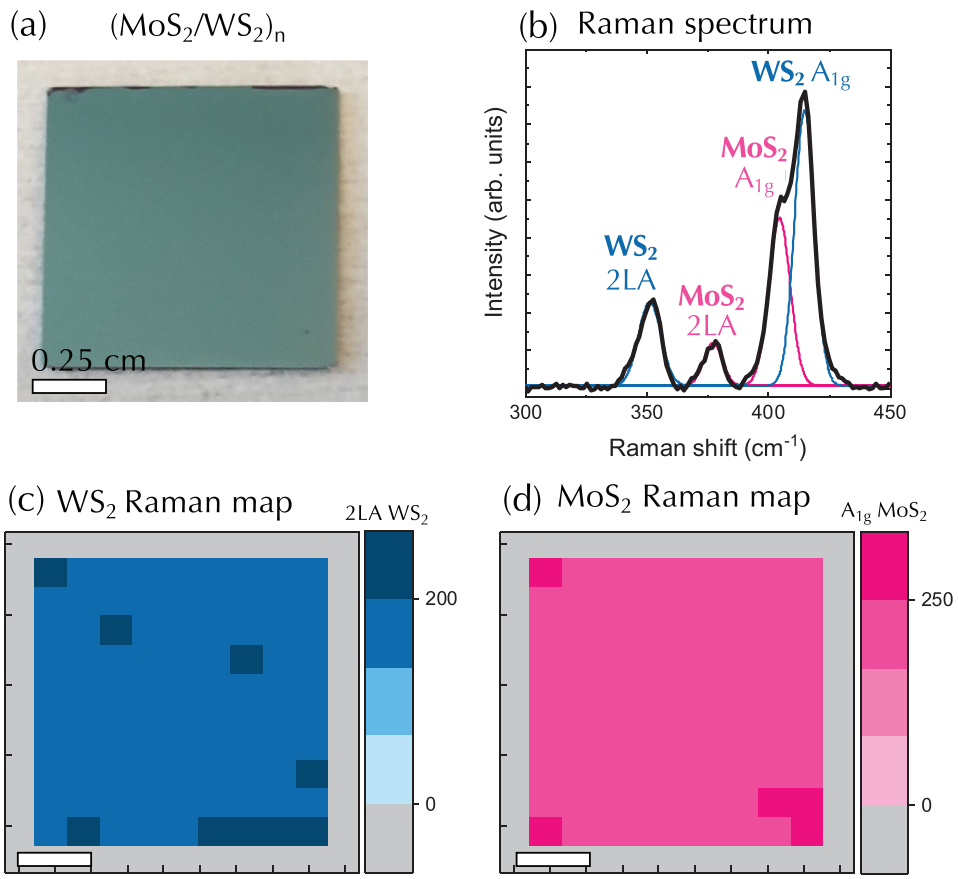

Figure 4. Large-scale Raman mapping of the superlattice. a) Optical observation of a cm^2 scale superlattice sample highlights high homogeneity. b) Raman spectroscopy reveals combined respective signatures of MoS_2 and WS_2 layers with MoS_2 2LA + E^1_{2g} modes, WS_2 2LA + E_{2g} modes, as well as the MoS_2 and WS_2 A_{1g}/A1′ modes. c,d) cm^2 scale mappings of the Raman response of WS_2 (2LA mode) and MoS_2 (A_{1g} mode) indicates full coverage. Scale bars in white are 0.25 cm.

have already been widely exploited in optoelectronics systems with more usual III-V semiconductors.[25–27,55–58] Starting in the 70s, with the early proposal by Esaki and Tsu of semiconductor superlattices[54] and the CVD synthesis by Blakeslee and Aliotta of GaAs based superlattices crystals[62] (closely followed by works with other approaches such as molecular beam epitaxy[63] and liquid phase epitaxy[64]), the field has bloomed toward modern electronics applications. In such superlattices, the constituent quantum wells are fabricated close enough to each other so their carrier work functions overlap and the composite material acquires its own band structure. 2D materials, beyond being the ultimate atomic building blocks for such layered heterostructures, could provide additional benefits to these systems. In particular, by nature all the chemical bonds of 2D semiconductors are maintained within the 2D layer, this relaxes the epitaxial growth with lattice matching conditions which are otherwise one of the key challenges to designing III–V heterostructures.[65] Alleviation of this concern allows us to envision a wide range of combinations within superlattices, associating the particularly large families of 2D semiconductors[8–11] ranging from elemental 2D materials (such as black phosphorus, silicene, germanene) to more complex layered compounds (such as mono-, bi- and trichalcogenides) to fine engineer relevant bandgap landscapes (as for more usual III-V superlattices[66]). This includes the possible exploitation of unique handles related to 2D materials, as their properties are closely related to their composition (as illustrated by large families of metal-chalcogens TMDs materials,[9] also extended by alloying[67] or Janus materials families[68]) and stackings twists (with impact on resulting band structures including more exotic phenomena such as “magic-angle” moiré induced superconductivity or ferroelectricity, as well as a wide range of topologically protected states[14–18]), leading to an even wider spectrum of available basic building blocks for the fabrication of 2D based superlattices. We however have to notice that the dramatic reduction of thickness unlocked by our approach, reaching combinations of atomically thin 2D layers, means that their properties deviate from expected bulk predictions due to exalted proximity effects.[12] In this ultimate thickness situation, 2D–2D interfaces fully drive the whole superlattice properties. This necessitates a meticulous examination of the specific bandgap landscape resulting from each engineered combination, as substantial deviation is anticipated reflecting the potential for emergent properties surpassing the mere sum of their constituent 2D elements. We believe that far from being a constrain on the applicability of these van der Waals superlattices, this interfacial hybridization of the 2D materials could provide an additional

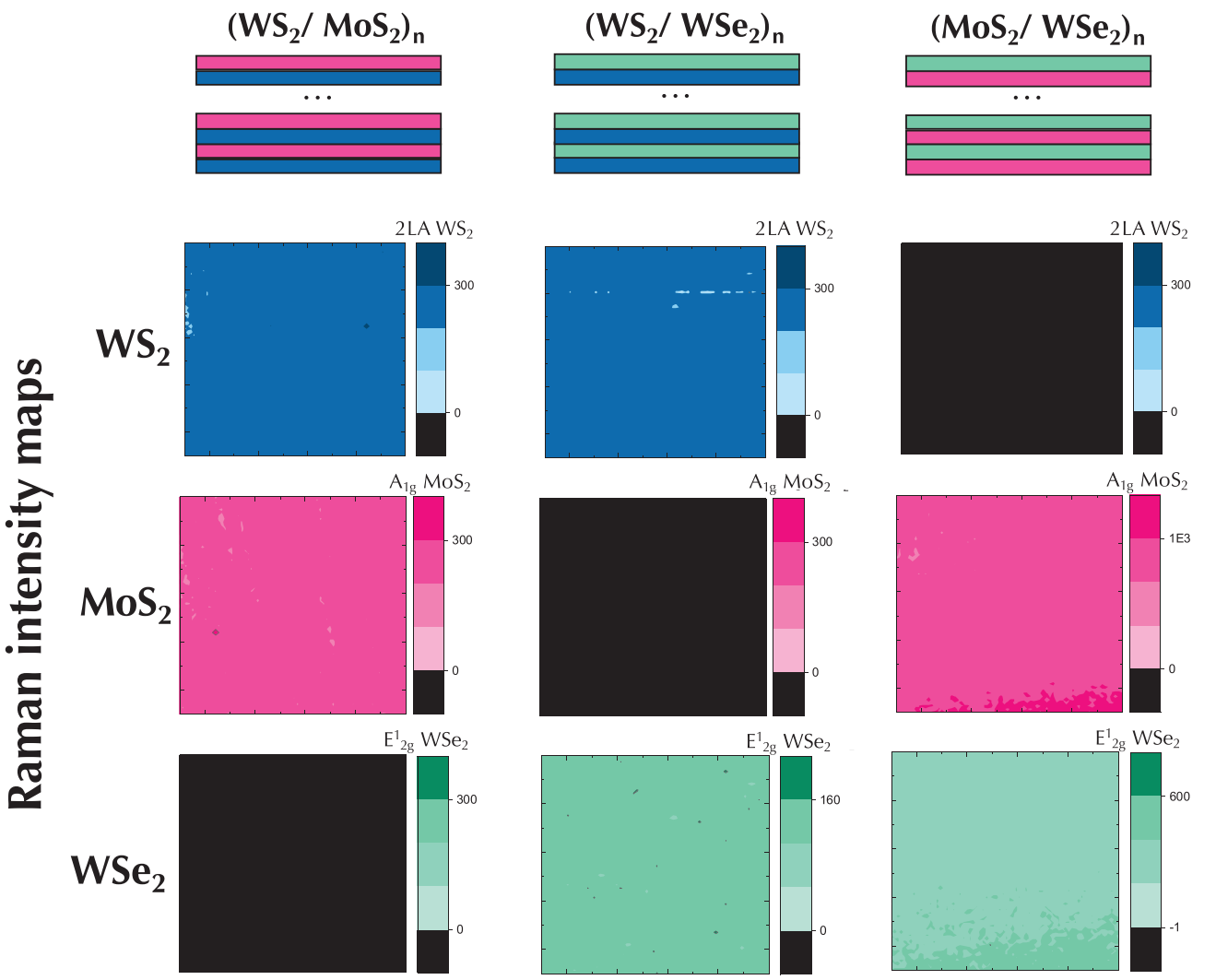

Figure 5. Analysis of the homogeneity of different artificial 2D superlattices $(MoS_2/WS_2)_n$, $(WS_2/WSe_2)_n$, and $(MoS_2/WSe_2)_n$ by Raman spectroscopy mappings. Large 45μm × 45μm Raman maps with 0.6 μm steps display the intensity of TMDs signature peaks (WS_2 2LA mode, MoS_2 A_{1g} mode, WSe_2 E^1_{2g} mode) for the various superlattice materials. Strikingly we observe a highly reproducible homogeneity of the different van der Waals materials derived by the PLD approach.

powerful handle to design the overall band structure and resulting modulations of the quantum confinements within the superlattice. However, going beyond general discussions of proximity effects' impact on superlattice band structures requires precise computations.

We discuss below the anticipated band structure landscape engineering opportunities of some TMDs superlattices, aiming to illustrate the general guideline that proximity effects are to be taken into account when stacking different 2D materials into large heterostructures. By blending the characteristics of the individual layers, proximity effects lead to the emergence of distinct properties once combined into complex van der Waals heterostructures. Group-VI TMDs (MX_2 with M = Mo, W and X = S, Se) are primarily found in the trigonal prismatic arrangement with the *2H* phase as the preferred polymorph.[69] In their bulk *2H* phase, these are characterized by indirect band gaps between the valence band maximum (VBM) at the center of the Brillouin zone (**Γ**), and the conduction band minimum (CBM) located at an intermediate point (Q) along the **Γ**–K path. The electronic band structure is sensitive to the inter-layer coupling and varies with the number of layers. When the crystal is thinned to a few layers, the inter-layer coupling decreases, and the conduction bands at Q move upward shifting the CBM to K while the valence bands at **Γ** moves downward shifting the VBM to K. Eventually, in the monolayer limit, group-VI TMDs reveal a direct band gap at the K-point.[70–75] Experimental evidence of this indirect to direct-gap transition has been provided by the observation of strongly enhanced photoluminescence in the monolayer limit.[8,76–78] When stacked into hetero-bilayers, Group-VI TMDs reveal a type-II alignment of the bands. The band offsets result from the work function and band gap differences between TMDs as well as from charge transfer and hybridization at the interfaces.[79,80–83] This has been observed both by microbeam X-ray photoelectron spectroscopy (*μ*-XPS) and scanning tunneling

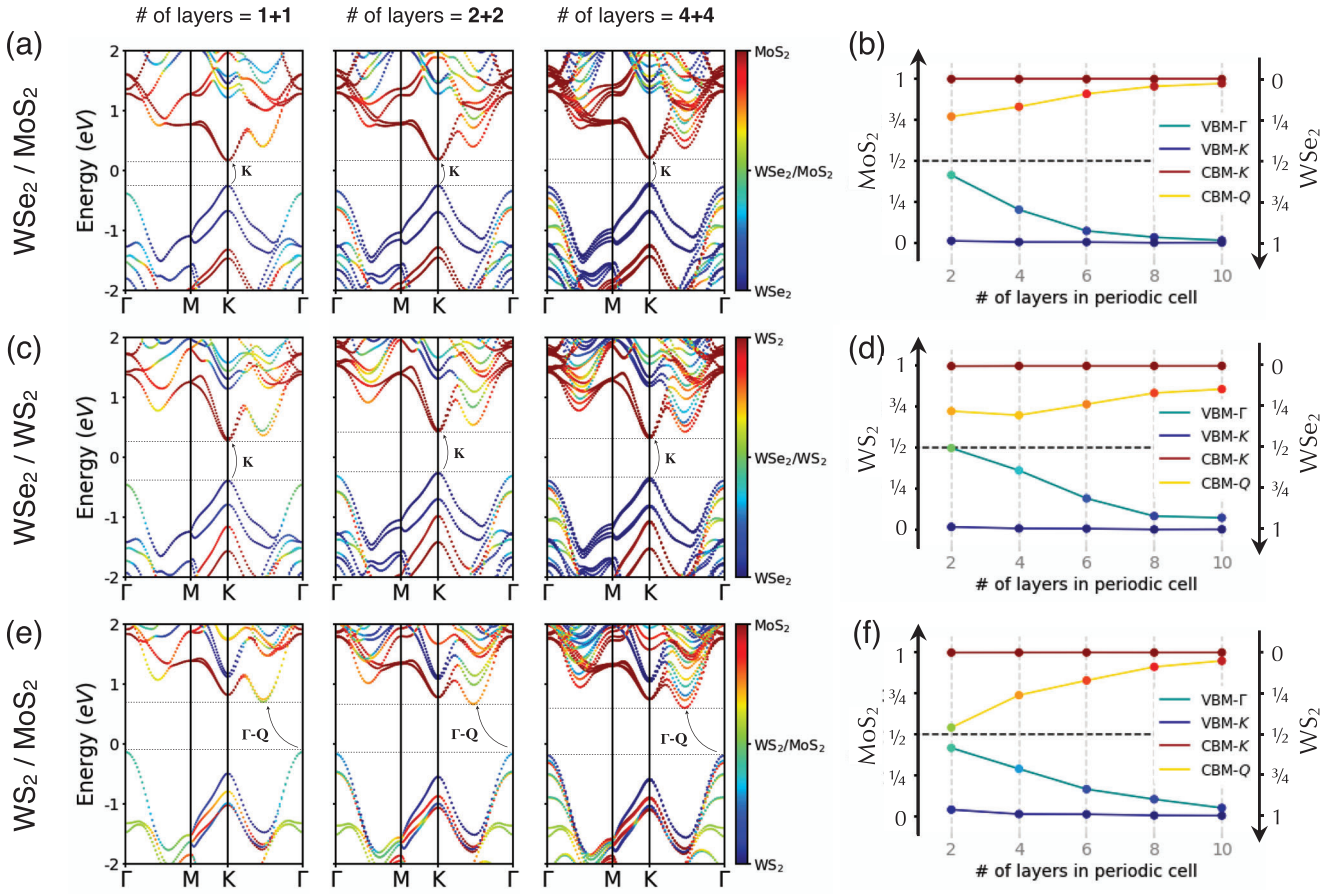

Figure 6. Computed electronic structures of van der Waals superlattices made of different periodic stacking of MoS_2, WS_2, and WSe_2. Band structures computed for various number of TMD layers in the periodic cell (# = 1 + 1, 2 + 2, 4 + 4) for the a) WSe_2/MoS_2, c) WSe_2/WS_2, e) WS_2/MoS_2 superlattices. The color is associated with the projection of the electronic eigenstates onto the constituting TMD slabs. Projections of the valence band maxima (VBM) at **Γ** and K, and the conduction band minima (CBM) at K and Q onto the constituting TMDs for b) WSe_2/MoS_2, d) WSe_2/WS_2, f) WS_2/MoS_2 superstructures with various number of TMD layers in the periodic cell. It appears that engineered hybridized interfacial states play a leading role in the ultra-thin limit regime.

spectroscopy (STS).[43,84] In agreement with theoretical predictions, direct band gaps at the K point have been observed in these systems with VBM and CBM spatially located in different layers.[12,43,83–87] The large electron-hole Coulomb interaction heterolayers and the spatially indirect nature of the electron-hole wavefunction provide interlayer excitons with interesting characteristics, such as long lifetimes, possible control by external fields, and valley-polarization inherited from the constitutive monolayers.[88,89]

Here, our focus is on the specific class of group-VI TMDs superlattices $((MX_2)_m/(M'X'_2)_m)$ made accessible by the PLD growth approach, for which we vary *m*, the number of layers of each TMD in the unit cell. Using first-principles calculations, we show that the electronic band structure of these novel hybrid crystals arises from the repetitive occurrence of type-II interfaces, which are modulated by interlayer coupling.

The electronic structure of the MoS_2/WSe_2 monolayer superlattice is illustrated in **Figure 6a**. The projection of the electronic wavefunctions on the MoS_2 and WSe_2 layers reveals a staggered alignment of the bands. The VBM and CBM are in the K-valleys. These valleys are characterized by weak interlayer hybridization and a clear spatial localization. The VBM wavefunctions are localized on WSe_2 while the CBM wavefunctions are localized on MoS_2. Valleys at **Γ** and Q points present much larger interlayer hybridization leading to periodicity-dependent delocalization of the wavefunctions across the MoS_2/WSe_2 interfaces. The delocalization, which is significant for a small number of layers, weakens as MoS_2 and WSe_2 get thicker and the superstructure becomes less dominated by interfaces (Figure 6b). The electronic structure of WS_2/WSe_2 superstructures (Figure 6c,d) is very similar. The main differences lie in the band offsets and the effective masses of the low-conduction bands. The electronic profile of MoS_2/WS_2 superlattices is, however, different (Figure 6e,f). Calculations reveal a staggered alignment of the bands, but with a predominant **Γ**-Q indirect gap similar to what is observed in bulk TMDs. This is a consequence of the interfacial coupling between the constitutive layers. Sharing the same chalcogen and presenting relatively small band offsets across the interface promote large interfacial hopping.[74,75] In this configuration, the VBM is located at the **Γ** and CBM is located at Q. Interlayer coupling is significant in the **Γ** and Q valleys and the wavefunctions

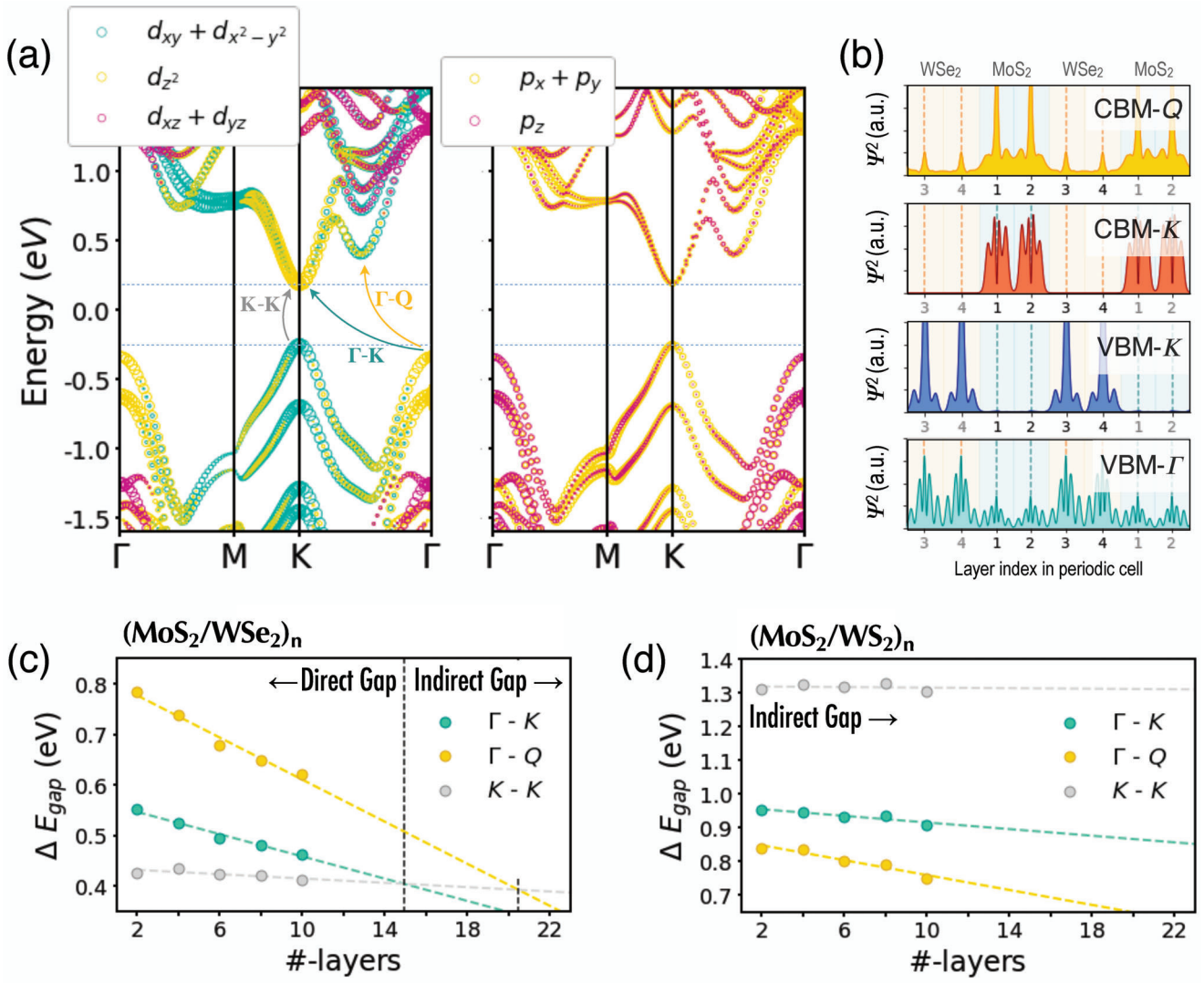

Figure 7. Direct or indirect nature of electronic gap of tailored mille-feuille superlattice material families. a) Orbital projected band structure of the WSe_2/MoS_2 superstructure with 2+2 TMD layers in unit-cell. Contributions from the metals (W and Mo) d-orbitals to the Bloch eigenstates are detailed on the left panel. Contributions from the chalcogens (Se and S) p-orbitals to the Bloch eigenstates are detailed on the right panel. b) The spatial resolution of the band edge wavefunctions: the valence band maxima (VBM) at **Γ** and K, and the conduction band minima (CBM) at K and Q) for the WSe_2/MoS_2 superstructures with 2+2 TMD layers in unit-cell. At K, the CBM and VBM are localized on the TMD layers of opposite slabs. At **Γ** and Q the VBM and CBM spread across the interfaces with a characteristic relative delocalization depending on the thickness of the slabs and the nature and strength of the interfacial coupling. The curve depicted has been obtained by integration of the electronic density associated with the wave function in the plane perpendicular to the epitaxial direction. c,d) Evolution of the direct and indirect electronic band gaps of the (c) WSe_2/MoS_2 and (d) WS_2/MoS_2 superstructures as a function of the number of TMD layers in unit cells. The location of the direct (K-K) and indirect (**Γ**-K and **Γ**-Q) gaps along the high symmetry paths in reciprocal space is depicted in (a). Dotted lines correspond to a linear extrapolation of first-principles results obtained by least square fitting. A direct-to-indirect crossover occurs for WSe_2/MoS_2 superlattices at ≈14 layers in the unit cell. WS_2/MoS_2 superlattices show an indirect band gap regardless of the number of TMD layers in the unit cell.

spread over the MoS_2/WS_2 interfaces instead of being localized independently on MoS_2 or WS_2.

The relative energies and spatial characteristics of the VBM and CBM states in the K-, **Γ**-, and Q-valleys rule the low-energy properties of this new class of superlattices. **Figure** 7a illustrates the orbital contributions to the low-energy wavefunctions of the superlattice family. The spatial resolution of the wavefunctions is pictured in Figure 7b. The lower energy bands at K primarily arise from a combination of the metals *d*-orbitals and the chalcogen *p*-orbitals. Specifically, the main contributions to the VBM stem from the metal $\{d_{xy}, d_{x^2-y^2}\}$ orbitals, while the CBM arises from the metal $\{d_{z^2}\}$ orbitals with minor contributions from the in-plane chalcogen $\{p_x, p_y\}$ orbitals. This results in a large SOC-induced energy splitting at VBM. SOC effectively suppresses interlayer hopping at the VBM and symmetry prevents it at the CBM, confining the band edge wavefunctions at the K point within the interfaces. Consequently, the physics of the CBM-K and VBM-K proceeds as if the constitutive TMD layers were

independent of each other as seen in Figure 7b. At **Γ** and Q, reduced SOC and a greater contribution of the p_z orbitals of the chalcogen facilitate interlayer hopping. Consequently, at VBM-**Γ** and CBM-Q, the band edge wavefunctions spread across the layers, as seen in Figure 7b. The spread depends on the slab composition, the thickness of the slab, and the nature and strength of the interfacial coupling.

The relative energies of the K-, **Γ**- and Q-valleys determine the nature of the energy gap. Direct gaps are pinned to the K-valleys and involve spatially confined states. Indirect gaps involve the **Γ**- and Q-valleys where wavefunctions present a tunable degree of delocalization. Figure 7c reports on the typical evolution of the direct and indirect band gaps in group-VI TMDs superlattices, exemplified here by the MoS_2/WSe_2 superstructures. The direct gap is primarily determined by the type-II alignment of the slabs. Its value is roughly independent of the number of TMD layers in the unit cell. On the contrary, the indirect gap decreases with increasing slab thicknesses. As TMD layers are added to the superstructure, the interlayer coupling gets stronger in each slab, pushing the **Γ** and Q-valleys closer to the fermi energy. Our first-principles calculations reveal a direct gap in the few-layer limit followed by a direct-to-indirect gap transition when increasing the slab thicknesses. In the limit of large slabs, the global VBM and CBM are predicted respectively in the **Γ**- and Q-valleys similar to what is observed in bulk TMDs. At these thicknesses, the superstructures are expected to be dominated by the physics of staggered bulk slabs. No direct to indirect gap transition is predicted in the MoS_2/WS_2 superstructures (Figure 7d) as the stronger interfacial interaction between the MoS_2 and WS_2 slab favors an indirect gap even in the few-layer limit.

In summary, we provide insight into the design possibilities enabled by tailoring van der Waals stacks using our PLD approach. Superlattices play a crucial role in advanced III-V applications, and 2D semiconductors offer a pathway to fabricate epitaxy-free heterostructures with precise atomic control, drawing from a wide array of 2D materials and combinations. While focusing on specific TMD superlattices systems, we highlight that one cannot directly extrapolate bulk or monolayer TMD properties to predict the electronic landscape. Depending on the particular composition and arrangement of the alternating slabs, the emergent electronic properties hinge on (i) the band structure of selected base materials and (ii) the hybridizations induced by interfacial coupling. This leads to the creation of unique quantum materials with engineered band-gap landscapes, offering a novel platform for fine-tuning the optoelectronic properties of TMDs heterostructures.

3. Conclusion

There are strong expectations for van der Waals systems expressed in the literature both from a fundamental point of view and in terms of potential applications (see for instance refs concerning photonics,[2,29] electronics,[1,3,5] spintronics[4]). While many van der Waals heterostructure properties are anticipated and discussed in the literature, experimental measurements have been limited to only a handful of accessible scenarios. Strikingly, while superlattices are fundamental to many applications such as quantum cascade lasers and are well-matured for III-V semiconductors,[25–27,55–58] they have never been fabricated out of 2D materials otherwise available for more than 15 years now. The primary obstacle lies in the fabrication process as there is no viable pathway beyond the labor-intensive methods of exfoliation and manual stackings which come with evident limitations such as limited layer counts (typically few layers) and an inherently ex-situ nature. Addressing this critical gap between expectations and methodology, this work opens an avenue to design well-defined artificial complex 2D van der Waals heterostructures over large surfaces, using an in-situ rapid direct PLD growth approach. A large number of repetitions of unit cells composed of different associated 2D semiconductors were fabricated over surfaces 8 orders of magnitudes larger than typical exfoliated 2D flakes, and on deposition timescales comparable to CMOS heterostructures of 3D materials grown by PVD approaches. This is to be compared to the incommensurable difficulty of stacking a few 2D layers by more usual wet transfer approaches or by pick-up-assisted mechanical exfoliation. Drawing from pioneering works in the field of 2D materials growth (see Ref.[9] for CVD growth of single TMD, as well as model studies for ex-situ 2–3 layers manual stackings[47,48]...), the provided characterizations underscore the superlattice configurations achieved in our study. TEM analysis reveals the intricate 2D layer stacking, XPS and EDX validate the anticipated chemical characteristics of both the 2D crystals and their stackings, and Raman spectroscopy highlights the crystalline nature of the resulting 2D layered materials. The tailoring potential of this approach is illustrated here through the exhibition of unique opportunities to pattern the band structure landscape (leveraging in particular on composition, layer count, and interfacial hybridization...) and we present precise staggered construction of various artificial superlattice semiconductors. Demonstrating complex van der Waals stacking designs is the first step (evocative of the early pioneering investigations into graphene growth[90]), providing an entry point to a community-wide exploration of anticipated complex van der Waals structures. We note in this direction that the PLD growth approach opens the door to epitaxial monocrystalline systems with a track record of success with multifunctional oxide systems.[91–93] Exploitation of tailorable in situ PLD approach specificities could lead to the identification of epitaxial or rotated van der Waals stackings, involving for instance varied growth kinetics with plume parameters and tailored combination of successive 2D materials with distinct lattice parameters. Overall, our study set a step in the direction of van der Waals lamellar quantum material tailoring, and the rapid exploration of their nanoelectronics, spintronics, and opto-electronics properties.

4. Experimental Section

TMD Superlattice Fabrication and Characterizations: Fabrications of the superlattices are carried in a TSST PLD chamber with a 1×10^{-8} mbar base vacuum. It is equipped with a Nd:YAG laser whose wavelength is reduced to 355 nm and the following ablation parameters are used: 80 mJ laser power, 7 ns pulse length, laser pulse frequency of 2.5 Hz. The distance between the target and the substrate is fixed at 70 mm allowing 2D-mode growth in the considered PLD conditions.[53] The 1 cm^2 SiO_2(90 nm)/Si substrates were inserted through a load lock and preheated at 400 °C in a 0.1 mbar Ar atmosphere before proceeding to growth. The targets are provided by Neyco with a fixed stoichiometry 1(W,Mo):2(S,Se) corresponding to aimed TMD unit materials, with purity >99.9%. They are shot under the same 0.1 mbar Ar atmosphere. After initial ex-situ preparation by surface

polishing and cleaning in isopropanol, each target is pre-ablated for 5 min in the PLD chamber before deposition, while the sample is protected behind a shutter. 2D semiconductor heterostructures are grown in a unique growth sequence without breaking the vacuum thanks to an in-situ target change system. To fabricate the superlattice, each 2D semiconductor layer is sequentially grown by ablation of a selected target during a usual deposition time of 20 s, while the sample temperature is kept at 400 °C. After the complete growth sequence, the samples are left to cool under 0.1 mbar Ar atmosphere for 1 h. They are then taken out for further characterization. For the TEM/EDX imaging, a Themis STEM setup is used from ThermoFisher Scientific, also equipped with a Super-X EDX detector, at 200 kV. XPS analysis of the superlattices is carried out using a Mg source and based on five spectra with 20 eV pass energy. Raman spectra and the different Raman mappings are taken with a Renishaw inVia 514 nm micro-Raman spectrometer.

First-Principles Electronic Structure Calculations: The electronic structures have been computed within the framework of Density Functional Theory (DFT)[94,95] using the projector augmented wave method (PAW) as implemented in the VASP code.[96,97] The exchange–correlation function is described using the Perdew–Burke–Ernzerhof (PBE) formulation of the generalized-gradient approximation.[98] The "GW" PAW potentials (v54) distributed with the code have been used. Tungsten and Molybden's semicore states were treated as valence orbitals. A $15 \times 15 \times 3$ Γ-centered k-point mesh is used for the Brillouin zone integrations of bulk TMDs in the 2H phase. Equivalently dense meshes are used in all calculations. The electron wave functions are expanded in a plane-wave basis set of 440 eV cutoff energy. The spin-orbit coupling has been included in the calculations in a self-consistent way. The van der Waals interactions are considered in the calculation of atomic forces and stress tensors by adding a correction term to the conventional DFT energy by means of the zero damping DFT-D3 method of Grimme et al.[99] All structures have been fully relaxed up to atomic forces <0.0001 eV $Å^{-1}$ and stress $<1 \times 10^{-5}$ eV $Å^{-3}$.

Acknowledgements

S.D. is the first author for the theoretical part. This project has received funding from the European Union's H2020 Future and Emerging Technologies Graphene Flagship (Grant Core3 No. 881603). This work was partly supported by the French RENATECH network. This research was supported by public grants overseen by the French National Research Agency (ANR) as part of the "Investissements d'Avenir" program Labex NanoSaclay (ANR-10-LABX-0035), as well as projects PEPR SPIN "SPINMAT" (ANR-22-EXSP-0007), PEPR ELEC "ADICT" (ANR-22-PEEL-0011), 2DTHERM (ANR-23-CE42-0015), and SWAG (ANR-23-CE24-0009). This research was also supported by the F.R.S.-FNRS through the research project "MOIRE" (N° T.029.22F), by the Fédération Wallonie-Bruxelles through ARC Grants (N° 21/26-116), by the EOS project "CONNECT" (N° 40007563), by the Flag-Era JTC project "MINERVA" (N° R.8006.21), and by the Pathfinder project "FLATS" (N° 101099139). Computational resources were provided by the supercomputing facilities of the Université Catholique de Louvain (CISM) and the Consortium des Equipements de Calcul Intensif en Fédération Wallonie Bruxelles (CECI) funded by the Fonds de la Recherche Scientifique de Belgique (F.R.S.-FNRS) under the convention N° 2.5020.11.

Conflict of Interest

The authors declare no conflict of interest.

Data Availability Statement

The data that support the findings of this study are available from the corresponding author upon reasonable request.

Keywords

2D semiconductors, pulsed laser deposition, quantum heterostructures, transition metal dichalcogenides, van der Waals heterostructures

Received: May 13, 2024
Published online:

[1] G. Fiori, F. Bonaccorso, G. Iannaccone, T. Palacios, D. Neumaier, A. Seabaugh, S. K. Banerjee, L. Colombo, *Nat. Nanotechnol.* **2014**, *9*, 768.
[2] D. Akinwande, C. Huyghebaert, C. H. Wang, M. I. Serna, S. Goossens, L. J. Li, H. S. P. Wong, F. H. L. Koppens, *Nature* **2019**, *573*, 507.
[3] M. C. Lemme, D. Akinwande, C. Huyghebaert, C. Stampfer, *Nat. Commun.* **2022**, *13*, 1392.
[4] H. Yang, S. O. Valenzuela, M. Chshiev, S. Couet, B. Dieny, B. Dlubak, A. Fert, K. Garello, M. Jamet, D.-E. Jeong, K. Lee, T. Lee, M.-B. Martin, G. S. Kar, P. Sénéor, H.-J. Shin, S. Roche, *Nature* **2022**, *606*, 663.
[5] G. Cao, P. Meng, J. Chen, H. Liu, R. Bian, C. Zhu, F. Liu, Z. Liu, *Adv. Funct. Mater.* **2021**, *31*, 2005443.
[6] S. Das, A. Sebastian, E. Pop, C. J. McClellan, A. D. Franklin, T. Grasser, T. Knobloch, Y. Illarionov, A. V. Penumatcha, J. Appenzeller, Z. Chen, W. Zhu, I. Asselberghs, L. J. Li, U. E. Avci, N. Bhat, T. D. Anthopoulos, R. Singh, *Nat. Electron.* **2021**, *4*, 786.
[7] A. Dodda, D. Jayachandran, A. Pannone, N. Trainor, S. P. Stepanoff, M. A. Steves, S. S. Radhakrishnan, S. Bachu, C. W. Ordonez, J. R. Shallenberger, J. M. Redwing, K. L. Knappenberger, D. E. Wolfe, S. Das, *Nat. Mater.* **2022**, *21*, 1379.
[8] K. F. Mak, C. Lee, J. Hone, J. Shan, T. F. Heinz, *Phys. Rev. Lett.* **2010**, *105*, 136805.
[9] J. Zhou, J. Lin, X. Huang, Y. Zhou, Y. Chen, J. Xia, H. Wang, Y. Xie, H. Yu, J. Lei, D. Wu, F. Liu, Q. Fu, Q. Zeng, C. H. Hsu, C. Yang, L. Lu, T. Yu, Z. Shen, H. Lin, B. I. Yakobson, Q. Liu, K. Suenaga, G. Liu, Z. Liu, *Nature* **2018**, *556*, E3.
[10] N. Mounet, M. Gibertini, P. Schwaller, D. Campi, A. Merkys, A. Marrazzo, T. Sohier, I. E. Castelli, A. Cepellotti, G. Pizzi, N. Marzari, *Nat. Nanotechnol.* **2018**, *13*, 246.
[11] M. Och, M. B. Martin, B. Dlubak, P. Seneor, C. Mattevi, *Nanoscale* **2021**, *13*, 2157.
[12] N. R. Wilson, P. v. Nguyen, K. Seyler, P. Rivera, A. J. Marsden, Z. P. L. Laker, G. C. Constantinescu, V. Kandyba, A. Barinov, N. D. M. Hine, X. Xu, D. H. Cobden, *Sci. Adv.* **2017**, *3*, e1601832.
[13] A. Chaves, J. G. Azadani, H. Alsalman, D. R. daCosta, R. Frisenda, A. J. Chaves, S. H. Song, Y. D. Kim, D. He, J. Zhou, A. Castellanos-Gomez, F. M. Peeters, Z. Liu, C. L. Hinkle, S. H. Oh, P. D. Ye, S. J. Koester, Y. H. Lee, P. Avouris, X. Wang, T. Low, *NPJ 2D Mater. Appl.* **2020**, *4*, 29.
[14] B. Hunt, J. D. Sanchez-Yamagishi, A. F. Young, M. Yankowitz, B. J. LeRoy, K. Watanabe, T. Taniguchi, P. Moon, M. Koshino, P. Jarillo-Herrero, R. C. Ashoori, *Science* **2013**, *340*, 1427.
[15] Y. Cao, V. Fatemi, S. Fang, K. Watanabe, T. Taniguchi, E. Kaxiras, P. Jarillo-Herrero, *Nature* **2018**, *556*, 43.
[16] P. Rickhaus, J. Wallbank, S. Slizovskiy, R. Pisoni, H. Overweg, Y. Lee, M. Eich, M. H. Liu, K. Watanabe, T. Taniguchi, T. Ihn, K. Ensslin, *Nano Lett.* **2018**, *18*, 6725.
[17] Z. Zheng, Q. Ma, Z. Bi, S. de la Barrera, M. H. Liu, N. Mao, Y. Zhang, N. Kiper, K. Watanabe, T. Taniguchi, J. Kong, W. A. Tisdale, R. Ashoori, N. Gedik, L. Fu, S. Y. Xu, P. Jarillo-Herrero, *Nature* **2020**, *588*, 71.
[18] L. Kou, Y. Ma, Z. Sun, T. Heine, C. Chen, *J. Phys. Chem. Lett.* **2017**, *8*, 1905.
[19] D. K. Polyushkin, S. Wachter, L. Mennel, M. Paur, M. Paliy, G. Iannaccone, G. Fiori, D. Neumaier, B. Canto, T. Mueller, *Nat. Electron.* **2020**, *3*, 486.

[20] K. Zhu, C. Wen, A. A. Aljarb, F. Xue, X. Xu, V. Tung, X. Zhang, H. N. Alshareef, M. Lanza, *Nat. Electron.* **2021**, *4*, 775.
[21] D. Neumaier, S. Pindl, M. C. Lemme, *Nat. Mater.* **2019**, *18*, 525.
[22] T. Schram, Q. Smets, B. Groven, M. Heyne, E. Kunnen, A. Thiam, K. Devriendt, A. Delabie, D. Lin, M. Lux, D. Chiappe, I. Asselberghs, S. Brus, C. Huyghebaert, S. Sayan, A. Juncker, M. Caymax, I. P. Radu, in *2017 47th European Solid-State Device Research Conference (ESSDERC)*, Editions Frontieres, Leuven, Belgium **2017**, pp. 212–215.
[23] P. Brus, V. Zatko, M. Galbiati, F. Godel, S. Collin, B. Servet, S. Xavier, R. Aubry, P. Garabedian, M. B. Martin, B. Dlubak, P. Seneor, O. Bezencenet, *Adv. Electron. Mater.* **2021**, *7*, 2001109.
[24] A. Piacentini, D. Marian, D. S. Schneider, E. González Marín, Z. Wang, M. Otto, B. Canto, A. Radenovic, A. Kis, G. Fiori, M. C. Lemme, D. Neumaier, *Adv. Electron. Mater.* **2022**, *8*, 2200123.
[25] F. Capasso, *Science* **1987**, *235*, 172.
[26] J. Faist, F. Capasso, D. L. Sivco, C. Sirtori, A. L. Hutchinson, A. Y. Cho, *Science* **1994**, *264*, 553.
[27] A. Nedelcu, C. Bonvalot, R. Taalat, J. Fantini, T. Colin, P. Muller, O. Huet, L. Dua, T. Laurent, C. Blin, A. le Priol, J. Coussement, M. Bettiati, P. Garabédian, *Infrared Phys. Technol.* **2018**, *94*, 273.
[28] Y. Liu, N. O. Weiss, X. Duan, H. C. Cheng, Y. Huang, X. Duan, *Nat. Rev. Mater.* **2016**, *1*, 16042.
[29] J. He, C. Wang, B. Zhou, Y. Zhao, L. Tao, H. Zhang, *Mater. Horiz.* **2020**, *7*, 2903.
[30] A. K. Geim, K. S. Novoselov, *Nat. Mater.* **2007**, *6*, 183.
[31] J. M. Woods, Y. Jung, Y. Xie, W. Liu, Y. Liu, H. Wang, J. J. Cha, *ACS Nano* **2016**, *10*, 2004.
[32] Y. Gong, J. Lin, X. Wang, G. Shi, S. Lei, Z. Lin, X. Zou, G. Ye, R. Vajtai, B. I. Yakobson, H. Terrones, M. Terrones, B. K. Tay, J. Lou, S. T. Pantelides, Z. Liu, W. Zhou, P. M. Ajayan, *Nat. Mater.* **2014**, *13*, 1135.
[33] Z. Cai, B. Liu, X. Zou, H. M. Cheng, *Chem. Rev.* **2018**, *118*, 6091.
[34] A. K. Geim, I. V. Grigorieva, *Nature* **2013**, *499*, 419.
[35] T. Iwasaki, K. Endo, E. Watanabe, D. Tsuya, Y. Morita, S. Nakaharai, Y. Noguchi, Y. Wakayama, K. Watanabe, T. Taniguchi, S. Moriyama, *ACS Appl. Mater. Interfaces* **2020**, *12*, 8533.
[36] Y. K. Luo, J. Xu, T. Zhu, G. Wu, E. J. McCormick, W. Zhan, M. R. Neupane, R. K. Kawakami, *Nano Lett.* **2017**, *17*, 3877.
[37] C. K. Safeer, J. Ingla-Aynés, F. Herling, J. H. Garcia, M. Vila, N. Ontoso, M. R. Calvo, S. Roche, L. E. Hueso, F. Casanova, *Nano Lett.* **2019**, *19*, 1074.
[38] A. M. Hoque, D. Khokhriakov, K. Zollner, B. Zhao, B. Karpiak, J. Fabian, S. P. Dash, *Commun. Phys.* **2021**, *4*, 124.
[39] A. Castellanos-Gomez, X. Duan, Z. Fei, H. R. Gutierrez, Y. Huang, X. Huang, J. Quereda, Q. Qian, E. Sutter, P. Sutter, *Nature Reviews Methods Primers* **2022**, *2*, 58.
[40] P. R. Kidambi, C. Ducati, B. Dlubak, D. Gardiner, R. S. Weatherup, M. B. Martin, P. Seneor, H. Coles, S. Hofmann, *J. Phys. Chem. C* **2012**, *116*, 22492.
[41] Y. Zhang, Y. Yao, M. G. Sendeku, L. Yin, X. Zhan, F. Wang, Z. Wang, J. He, *Adv. Mater.* **2019**, *31*, 1901694.
[42] N. Briggs, S. Subramanian, Z. Lin, X. Li, X. Zhang, K. Zhang, K. Xiao, D. Geohegan, R. Wallace, L. Q. Chen, M. Terrones, A. Ebrahimi, S. Das, J. Redwing, C. Hinkle, K. Momeni, A. van Duin, V. Crespi, S. Kar, J. A. Robinson, *2D Mater.* **2019**, *6*, 022001.
[43] M. H. Chiu, C. Zhang, H. W. Shiu, C. P. Chuu, C. H. Chen, C. Y. S. Chang, C. H. Chen, M. Y. Chou, C. K. Shih, L. J. Li, *Nat. Commun.* **2015**, *6*, 7666.
[44] V. Zatko, S. M. M. Dubois, F. Godel, C. Carrétéro, A. Sander, S. Collin, M. Galbiati, J. Peiro, F. Panciera, G. Patriarche, P. Brus, B. Servet, J. C. Charlier, M. B. Martin, B. Dlubak, P. Seneor, *ACS Nano* **2021**, *15*, 7279.
[45] M. Galbiati, V. Zatko, F. Godel, P. Hirschauer, A. Vecchiola, K. Bouzehouane, S. Collin, B. Servet, A. Cantarero, F. Petroff, M. B. Martin, B. Dlubak, P. Seneor, *ACS Appl. Electron Mater.* **2020**, *2*, 3508.
[46] S. Pace, L. Martini, D. Convertino, D. H. Keum, S. Forti, S. Pezzini, F. Fabbri, V. Mišeikis, C. Coletti, *ACS Nano* **2021**, *15*, 4213.
[47] J. H. Kim, T. J. Ko, E. Okogbue, S. S. Han, M. S. Shawkat, M. G. Kaium, K. H. Oh, H. S. Chung, Y. Jung, *Sci. Rep.* **2019**, *9*, 1641.
[48] S. S. Han, T. J. Ko, C. Yoo, M. S. Shawkat, H. Li, B. K. Kim, W. K. Hong, T. S. Bae, H. S. Chung, K. H. Oh, Y. Jung, *Nano Lett.* **2020**, *20*, 3925.
[49] K. E. Aretouli, D. Tsoutsou, P. Tsipas, J. Marquez-Velasco, S. Aminalragia Giamini, N. Kelaidis, V. Psycharis, A. Dimoulas, *ACS Appl. Mater. Interfaces* **2016**, *8*, 23222.
[50] N. Choudhary, J. Park, J. Y. Hwang, H.-S. Chung, K. H. Dumas, S. I. Khondaker, W. Choi, Y. Jung, *Sci. Rep.* **2016**, *6*, 25456.
[51] S. Seo, I. Oh, J.-C. Park, J. Lee, Y. Jung, H. Choi, J. Ryu, S. Lee, *ACS Appl. Nano Mater.* **2021**, *4*, 12017.
[52] L. Khalil, D. Pierucci, E. Velez-Fort, J. Avila, C. Vergnaud, P. Dudin, F. Oehler, J. Chaste, M. Jamet, E. Lhuillier, M. Pala, A. Ouerghi, *Nanotechnology* **2022**, *34*, 045702.
[53] F. Godel, V. Zatko, C. Carrétéro, A. Sander, M. Galbiati, A. Vecchiola, P. Brus, O. Bezencenet, B. Servet, M. B. Martin, B. Dlubak, P. Seneor, *ACS Appl. Nano Mater.* **2020**, *3*, 7908.
[54] L. Esaki, R. Tsu, *IBM J. Res. Dev.* **1970**, *14*, 61.
[55] B. F. Levine, *J. Appl. Phys.* **1993**, *74*, R1.
[56] L. Gendron, M. Carras, A. Huynh, V. Ortiz, C. Koeniguer, V. Berger, *Appl. Phys. Lett.* **2004**, *85*, 2824.
[57] L. De Santis, C. Antón, B. Reznychenko, N. Somaschi, G. Coppola, J. Senellart, C. Gómez, A. Lemaître, I. Sagnes, A. G. White, L. Lanco, A. Auffèves, P. Senellart, *Nat. Nanotechnol.* **2017**, *12*, 663.
[58] P. Senellart, G. Solomon, A. White, *Nat. Nanotechnol.* **2017**, *12*, 1026.
[59] T. A. J. Loh, D. H. C. Chua, A. T. S. Wee, *Sci. Rep.* **2015**, *5*, 18116.
[60] A. Berkdemir, H. R. Gutiérrez, A. R. Botello-Méndez, N. Perea-López, A. L. Elías, C. I. Chia, B. Wang, V. H. Crespi, F. López-Urías, J. C. Charlier, H. Terrones, M. Terrones, *Sci. Rep.* **2013**, *3*, 1755.
[61] P. Tonndorf, R. Schmidt, P. Böttger, X. Zhang, J. Börner, A. Liebig, M. Albrecht, C. Kloc, O. Gordan, D. R. T. Zahn, S. Michaelis de Vasconcellos, R. Bratschitsch, *Opt. Express* **2013**, *21*, 4908.
[62] A. E. Blakeslee, C. F. Aliotta, *IBM J. Res. Dev.* **1970**, *14*, 686.
[63] A. Y. Cho, *Appl. Phys. Lett.* **1971**, *19*, 467.
[64] J. M. Woodall, *J. Cryst. Growth* **1972**, *12*, 32.
[65] T. F. Kuech, *Prog. Cryst. Growth Charact. Mater.* **2016**, *62*, 352.
[66] M. Fox, R. Ispasoiu, in *Springer Handbook of Electronic and Photonic Materials*, (Eds.: S. Kasp, P. Capper), Springer, Berlin, **2017**, p. 1037.
[67] L. M. Xie, *Nanoscale* **2015**, *7*, 18392.
[68] L. Zhang, Y. Xia, X. Li, L. Li, X. Fu, J. Cheng, R. Pan, *J. Appl. Phys.* **2022**, *131*, 230902.
[69] M. Chhowalla, H. S. Shin, G. Eda, L. J. Li, K. P. Loh, H. Zhang, *Nat. Chem.* **2013**, *5*, 263.
[70] Y. Sun, D. Wang, Z. Shuai, *J. Phys. Chem. C* **2016**, *120*, 21866.
[71] R. Roldán, J. A. Silva-Guillén, M. P. López-Sancho, F. Guinea, E. Cappelluti, P. Ordejón, *Ann. Phys.* **2014**, *526*, 347.
[72] W. S. Yun, S. W. Han, S. C. Hong, I. G. Kim, J. D. Lee, *Phys. Rev. B* **2012**, *85*, 033305.
[73] Y. Liang, S. Huang, R. Soklaski, L. Yang, *Appl. Phys. Lett.* **2013**, *103*, 042106.
[74] G. bin Liu, D. Xiao, Y. Yao, X. Xu, W. Yao, *Chem. Soc. Rev.* **2015**, *44*, 2643.
[75] E. Cappelluti, R. Roldán, J. A. Silva-Guillén, P. Ordejón, F. Guinea, *Phys. Rev. B Condens. Matter Mater. Phys.* **2013**, *88*, 075409.
[76] A. Splendiani, L. Sun, Y. Zhang, T. Li, J. Kim, C. Y. Chim, G. Galli, F. Wang, *Nano Lett.* **2010**, *10*, 1271.
[77] Y. Zhang, T. R. Chang, B. Zhou, Y. T. Cui, H. Yan, Z. Liu, F. Schmitt, J. Lee, R. Moore, Y. Chen, H. Lin, H. T. Jeng, S. K. Mo, Z. Hussain, A. Bansil, Z. X. Shen, *Nat. Nanotechnol.* **2013**, *9*, 111.
[78] W. Zhao, Z. Ghorannevis, L. Chu, M. Toh, C. Kloc, P. H. Tan, G. Eda, *ACS Nano* **2013**, *7*, 791.

[79] J. Kang, S. Tongay, J. Zhou, J. Li, J. Wu, *Appl. Phys. Lett.* **2013**, *102*, 012111.
[80] Y. Guo, J. Robertson, *Appl. Phys. Lett.* **2016**, *108*, 233104.
[81] V. O. Özçelik, J. G. Azadani, C. Yang, S. J. Koester, T. Low, *Phys. Rev. B* **2016**, *94*, 035125.
[82] C. Zhang, C. Gong, Y. Nie, K. A. Min, C. Liang, Y. J. Oh, H. Zhang, W. Wang, S. Hong, L. Colombo, R. M. Wallace, K. Cho, *2D Mater.* **2016**, *4*, 015026.
[83] H. P. Komsa, A. V. Krasheninnikov, *Phys. Rev. B Condens Matter Mater. Phys.* **2013**, *88*, 085318.
[84] C. Quan, C. Lu, C. He, X. Xu, Y. Huang, Q. Zhao, X. Xu, *Adv. Mater. Interfaces* **2019**, *6*, 1801733.
[85] P. Rivera, J. R. Schaibley, A. M. Jones, J. S. Ross, S. Wu, G. Aivazian, P. Klement, K. Seyler, G. Clark, N. J. Ghimire, J. Yan, D. G. Mandrus, W. Yao, X. Xu, *Nat. Commun.* **2015**, *6*, 6242.
[86] B. Amin, N. Singh, U. Schwingenschlögl, *Phys. Rev. B Condens Matter Mater. Phys.* **2015**, *92*, 075439.
[87] D. A. Ruiz-Tijerina, V. I. Fal'Ko, *Phys. Rev. B* **2019**, *99*, 125424.
[88] P. Rivera, H. Yu, K. L. Seyler, N. P. Wilson, W. Yao, X. Xu, *Nat. Nanotechnol.* **2018**, *13*, 1004.
[89] C. Jin, E. Y. Ma, O. Karni, E. C. Regan, F. Wang, T. F. Heinz, *Nat. Nanotechnol.* **2018**, *13*, 994.
[90] A. Reina, X. Jia, J. Ho, D. Nezich, H. Son, V. Bulovic, M. S. Dresselhaus, K. Jing, *Nano Lett.* **2009**, *9*, 30.
[91] V. Garcia, M. Bibes, L. Bocher, S. Valencia, F. Kronast, A. Crassous, X. Moya, S. Enouz-Vedrenne, A. Gloter, D. Imhoff, C. Deranlot, N. D. Mathur, S. Fusil, K. Bouzehouane, A. Barthélémy, *Science* **2010**, *327*, 1106.
[92] A. Chanthbouala, A. Crassous, V. Garcia, K. Bouzehouane, S. Fusil, X. Moya, J. Allibe, B. Dlubak, J. Grollier, S. Xavier, C. Deranlot, A. Moshar, R. Proksch, N. D. Mathur, M. Bibes, A. Barthélémy, *Nat. Nanotechnol.* **2012**, *7*, 101.
[93] J. M. De Teresa, A. Barthélémy, A. Fert, J. P. Contour, F. Montaigne, P. Seneor, *Science* **1999**, *286*, 507.
[94] P. Hohenberg, W. Kohn, *Phys. Rev.* **1964**, *136*, B864.
[95] W. Kohn, L. J. Sham, *Phys. Rev.* **1965**, *140*, A1133.
[96] G. Kresse, J. Furthmüller, *Phys. Rev. B* **1996**, *54*, 11169.
[97] G. Kresse, D. Joubert, *Phys. Rev. B* **1999**, *59*, 1758.
[98] J. P. Perdew, K. Burke, M. Ernzerhof, *Phys. Rev. Lett.* **1996**, *77*, 3865.
[99] S. Grimme, J. Antony, S. Ehrlich, H. Krieg, *J. Chem. Phys.* **2010**, *132*, 154104.